

## SHORT-TERM VARIABILITY AND PSD ANALYSIS OF THE RADIO-LOUD AGN 3C 390.3

MARIO GLIOZZI

George Mason University, 4400 University Drive, Fairfax, VA 22030

IOSSIF E. PAPADAKIS

Physics Department, University of Crete, Greece

MICHAEL ERACLEOUS<sup>1</sup>

Department of Astronomy & Astrophysics, The Pennsylvania State University, 525 Davey Lab, University Park, PA 16802

RITA M. SAMBRUNA

NASA's Goddard Space Flight Center, Code 661, Greenbelt, MD 20771

DAVID R. BALLANTYNE

Department of Physics, The University of Arizona, 1118 East 4th Street, Tucson, AZ 85721

VALENTINA BRAITO

Department of Physics and Astronomy, University of Leicester, Leicester LE1 7RH, UK

JAMES N. REEVES

Astrophysics Group, School of Physical and Geographical Sciences, Keele University, Keele, Staffordshire, UK

*Draft version October 25, 2018*

### ABSTRACT

We investigate the short-term variability properties and the power spectral density (PSD) of the Broad-Line Radio Galaxy (BLRG) 3C 390.3 using observations made by *XMM-Newton*, *RXTE*, and *Suzaku* on several occasions between October 2004 and December 2006. The main aim of this work is to derive model-independent constraints on the origin of the X-ray emission and on the nature of the central engine in 3C 390.3. On timescales of the order of few hours, probed by uninterrupted *XMM-Newton* light curves, the flux of 3C 390.3 is consistent with being constant in all energy bands. On longer timescales, probed by the 2-day *RXTE* and *Suzaku* observations, the flux variability becomes significant. The latter observation confirms that the spectral variability behavior of 3C 390.3 is consistent with the spectral evolution observed in (radio-quiet) Seyfert galaxies: the spectrum softens as the source brightens. The correlated variability between soft and hard X-rays, observed during the *Suzaku* exposure and between the 2 *XMM-Newton* pointings, taken 1 week apart, argues against scenarios characterized by the presence of two distinct variable components in the 0.5–10 keV X-ray band. A detailed PSD analysis carried out over five decades in frequency suggests the presence of a break at  $T_{br} = 43^{+34}_{-25}$  days at a 92% confidence level. This is the second tentative detection of a PSD break in a radio-loud, non-jet dominated AGN, after the BLRG 3C 120, and appears to be in general agreement with the relation between  $T_{br}$ ,  $M_{BH}$ , and  $L_{bol}$ , followed by Seyfert galaxies. Our results indicate that the X-ray variability properties of 3C 390.3 are broadly consistent with those of radio-quiet AGN, suggesting that the X-ray emission mechanism in 3C 390.3 is similar to that of nearby Seyfert galaxies without any significant contribution from a jet component.

*Subject headings:* Galaxies: active – Galaxies: nuclei – X-rays: galaxies

### 1. INTRODUCTION

Relativistic bipolar outflows, generally emitting most of their energy in the radio range, are one of the most dramatic manifestations of the presence of supermassive black holes in Active Galactic Nuclei (AGN). Although it is widely accepted that these ejections are closely related to the accretion process onto the central black hole, the details of this link are still unknown.

A promising approach for tackling this problem is to investigate the X-ray properties of AGN with jets (generally called radio-loud AGN) and carry out a systematic comparison with their radio-quiet counterparts, the Seyfert galaxies. Unlike optical and UV light, X-rays are not significantly attenuated and are less affected by dilution from the host galaxy and are thought to be produced in the inner most regions of the accretion flow, thus may provide the most direct view of the central engine.

Broad-line radio galaxies (hereafter BLRGs) are one of the best classes of radio-loud AGN for this compara-

<sup>1</sup> Center for Gravitational Wave Physics, The Pennsylvania State University, University Park, PA 16802

tive analysis; they have optical and UV spectral properties similar to Seyfert galaxies, but they also host large-scale radio jets that are absent in their radio-quiet counterparts. Past X-ray spectroscopic studies, employing *ASCA*, *RXTE* and *BeppoSAX* data, have shown that BLRGs have weak Fe  $K\alpha$  lines and weak or absent Compton reflection humps at energies  $\gtrsim 10$  keV, a hallmark of Seyfert 1 galaxies (e.g., Woźniak et al. 1998; Sambruna et al. 1999; Eracleous et al. 2000; Zdziarski & Grandi 2001; Grandi et al. 2006). These findings have been confirmed by recent studies that made use of higher quality spectra provided by *Chandra* and *XMM-Newton* (e.g., Ballantyne et al. 2004, Ballantyne 2005; Ogle et al. 2004; Lewis et al. 2005; Gliozzi et al. 2007). Indeed, the weakness of the Fe  $K\alpha$  line and the Compton reflection continuum are very important observational clues, since they represent a major difference between radio-loud and radio-quiet AGN. However, the origin of this difference is still debated (see Gliozzi et al. 2007 for a detailed discussion on the competing models).

The importance of temporal studies lies in that they may provide model-independent information that complements the findings from spectral studies and possibly breaks the spectral degeneracy. Indeed, the similarity of the temporal and spectral variability properties of 2 BLRGs (including 3C 390.3) with those of Seyfert galaxies, led us to rule out a jet origin for the bulk of X-ray flux from these BLRGs and provided tight constraints on the jet contribution (Gliozzi et al. 2003a).

Past temporal studies indicate that the flux variability of 3C 390.3 is associated with spectral variability, in the sense that the spectrum softens as the flux increases. The presence of flux and spectral variability has been observed separately in the 2–15 keV band with *RXTE* (Gliozzi et al. 2003a, 2006), in the 2–10 keV energy band using *ASCA* and *Ginga* (Leighly et al. 1997), as well as at softer energies (0.1–2.4 keV) with *ROSAT* (Leighly et al. 1997). Importantly, all the above results, are based either on long-term (months to years) monitoring campaigns or on multiple observations spanning several years, but none addresses specifically the short-term variability. Although in the literature there are several studies based on individual observations of 3C 390.3 with different X-ray satellites (e.g., *EXOSAT* from Inda et al. 1994; *ASCA* from Eracleous et al. 1996, or *BeppoSAX* from Grandi et al. 1999), they all are focused on the spectral analysis and the temporal analysis is generally limited to few sentences indicating that the flux appears to be constant on timescales shorter than 1 day.

The apparent absence of short-term variability in 3C 390.3 seems to be in line with scaling relations inferred from power spectral density studies of radio-quiet AGN (see McHardy et al. 2006 and references therein). However, the lack of short-term variability in this AGN has never been tested by a satellite with the capabilities of *XMM-Newton*, which combines a very high throughput with highly elliptical orbits. These capabilities produce high quality uninterrupted light curves that have revealed the presence of short-term variability also in unexpected AGN classes, such as LINERs or low-luminosity Seyfert galaxies (e.g., Gliozzi et al. 2003b, 2008; Papadakis et al. 2009).

Taking advantage of the unique capabilities of *XMM-Newton* we perform for the first time a thorough analysis

of the temporal and spectral variability of 3C 390.3 on timescales of a few hours. This study is complemented by a similar analysis on timescales of 2 days, based on high quality variability data from *Suzaku* and from *RXTE*. These data are then combined with long-term *RXTE* monitoring data to produce the first power spectral density (PSD) of 3C 390.3. A detailed analysis of the time-averaged spectral properties is reported in a companion paper by Sambruna et al. (2009) and can be summarized as follows: 1) the broad-band 0.4–100 keV continuum is well described by a power law with  $\Gamma = 1.6$  and a high-energy cut-off at  $E_{\text{cutoff}} = 175$  keV; 2) reprocessing by two different “reflectors” (one neutral with  $R = 0.5$  and one ionized with  $\xi \simeq 2700$ ) is required; 3) the Fe  $K\alpha$  line profile is well fitted by a narrow component centered at 6.4 keV plus a broad component at 6.6 keV (apparently from He-like Fe).

This paper is organized as follows. In § 2 we describe the observations and data reduction. The short timescale (from few hours to 2 days) flux and spectral variability analyses are reported in § 3 and § 4, respectively. In § 5 we perform a PSD analysis combining the short-time scale light curves from this paper with long-time scale light curves from past *RXTE* monitoring campaigns. In § 6 we discuss the main results, and finally in § 7 we summarize the main conclusions. Hereafter, we adopt  $H_0 = 71$  km s $^{-1}$  Mpc $^{-1}$ ,  $\Omega_\Lambda = 0.73$  and  $\Omega_M = 0.27$  (Bennet et al. 2003); with the assumed cosmological parameters, the luminosity distance of 3C 390.3 ( $z=0.056$ ) is 247 Mpc. For the temporal analysis we make use of the  $\chi^2$  test to assess the significance of the variability and consider a light curve significantly variable if the probability of the null hypothesis (i.e., the source being constant) is less than 1%.

## 2. OBSERVATIONS AND DATA REDUCTION

We observed 3C 390.3 with *XMM-Newton* on 2004 October 10 and 17 for 50 ks and 20 ks, respectively. All of the EPIC cameras (Strüder et al. 2001; Turner et al. 2001) were operated in small window mode to prevent photon pile-up, and with medium filters, due to the presence of bright nearby sources in the field of view. The data reduction has been performed following the standard procedure with the *XMM-Newton* Science Analysis Software (SAS) 7.1; a detailed description is given in Sambruna et al. (2009).

### 2.1. *XMM-Newton*

In order to cover the harder part of the X-ray band, up to 40 keV, 3C 390.3 was also observed by *RXTE*. Unfortunately, the *RXTE* coverage, which was intended to be simultaneous to the *XMM-Newton* observations, was carried out on 2005 January 12 and 13, i.e. nearly two months after the *XMM-Newton* observations, due to scheduling problems. Because of the well known long-term temporal and spectral variability of 3C 390.3, the *RXTE* data cannot be safely combined with the EPIC data for a broadband spectral analysis. Nevertheless, the *RXTE* observation, which has a total exposure of 80 ks spanning a 2-day interval, is useful for investigating the variability on intermediate timescales at higher energies.

The *RXTE* observations (both the new observations presented here and the older observations used for the PSD analysis) were carried out with the Proportional

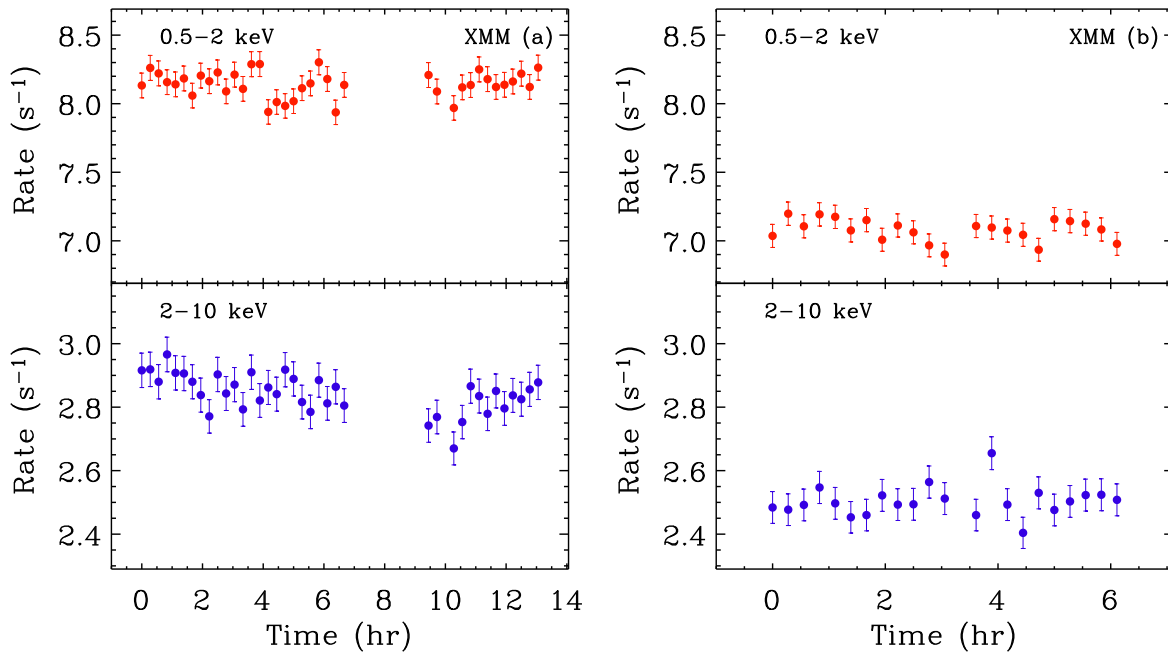


FIG. 1.— *Left:* *XMM-Newton* EPIC pn light curves of the soft (0.5–2 keV) and hard count rate (2–10 keV) on 2004 October 10. Time bins of 1000 s have been used. *Right:* *XMM-Newton* EPIC light curves light curves on 2004 October 17.

Counter Array (PCA; Jahoda et al. 1996), and the High-Energy X-Ray Timing Experiment (HEXTE; Rothschild et al. 1998) instruments. Here we will consider only PCA data, because the signal-to-noise ratio (hereafter S/N) of the HEXTE data is too low for a meaningful analysis. The PCA data were screened according to the following acceptance criteria: the satellite was out of the South Atlantic Anomaly (SAA) for at least 30 minutes, the Earth elevation angle was  $\geq 10^\circ$ , the offset from the nominal optical position was  $\leq 0.02^\circ$ , and the parameter ELECTRON-2 was  $\leq 0.1$ . The last criterion excludes data with high particle background rates in the Proportional Counter Units (PCUs). The PCA background light curves were determined using the L7 – 240 model developed at the *RXTE* Guest Observer Facility (GOF). This model is implemented by the program `pcabackest` v.2.1b and is applicable to “faint” sources, i.e., those with count rates  $< 40\text{s}^{-1}\text{PCU}^{-1}$ . All the above tasks were carried out with the help of the `REX` script provided by the *RXTE* GOF, which calls the relevant programs from the `FTOOLS` v.6.5 software package and also produces response matrices and effective area curves for the specific time of the observation. Data were initially extracted with 16 s time resolution and then re-binned to different bin widths for different applications. The short-term temporal analysis is restricted to PCA, STANDARD-2 mode, 2–15 keV, Layer 1 data, because that is where the PCA is best calibrated and most sensitive. For the PSD study we restricted the analysis to the 2–10 keV energy band, since this is the common energy range for *RXTE*, *Suzaku*, and *XMM-Newton*. PCUs 0 and 2 were turned on throughout the monitoring campaign. However, since the propane layer on PCU0 was damaged in May 2000, causing a systematic increase of the background, we conservatively use only PCU2 for our analysis. All quoted

count rates are therefore for one PCU.

*Suzaku* observed 3C 390.3 on 2006 December 14–16 for a total exposure time of 100 ks. We used the cleaned event files obtained from version 2 of the *Suzaku* pipeline processing, according to standard screening criteria. The XIS0, XIS1, and XIS3 source light curves were extracted from circular regions of radius 2.9 centered on the source and combined in order to increase the S/N; background light curves were extracted from four circular regions offset from the source. For the HXD-PIN data reduction and analysis we followed the latest *Suzaku* data reduction guide, and used the rev2 data, which include all the 4 cluster units and the best background available, model D, which has a systematic uncertainty of  $\pm 1.3\%$  at  $1\sigma$  level<sup>2</sup>. See Sambruna et al. (2008) for a more detailed description of the *Suzaku* data reduction.

### 3. SHORT-TIME SCALE FLUX VARIABILITY

Figures 1a and 1b show the EPIC pn light curves of the soft (0.5–2 keV; top panels) and hard (2–10 keV; bottom panels) count rate on 2004 October 10 and October 17. Hereafter, for the sake of simplicity, we will refer to the 2 *XMM-Newton* pointings as observations A and B, respectively. The average 2–10 keV fluxes during these two observations were  $3.9 \times 10^{-11}$  and  $3.4 \times 10^{-11}\text{erg cm}^{-2}\text{s}^{-1}$ , respectively. In order to allow a direct comparison between observations A and B, we have kept the same vertical scales in Fig. 1a and b. In this way, the significant decrease in count rate is easily discernible. Specifically, between the first and the second exposure, the EPIC pn average count rate decreases from  $10.99 \pm 0.01\text{s}^{-1}$  to  $9.58 \pm 0.01\text{s}^{-1}$  in the 0.5–10 keV energy band. A visual inspection of Fig. 1 suggests that, despite the presence

<sup>2</sup> <ftp://legacy.gsfc.nasa.gov/suzaku/doc/hxd/suzakumemo-2008-03.pdf>

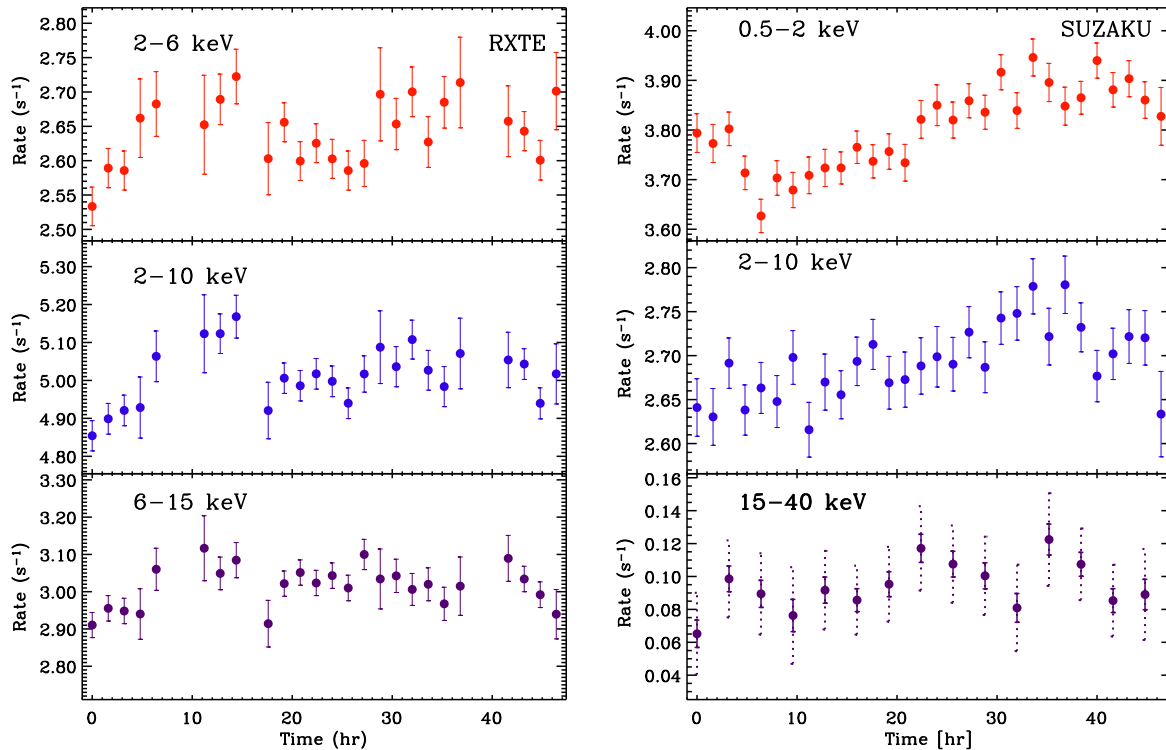


FIG. 2.— *Left*: *RXTE* PCA light curves in the 2–6 keV, 2–10 keV and 6–15 keV energy bands. Time bins of 5760 s ( $\sim 1$  *RXTE* orbit) have been used. *Right*: *Suzaku* XIS013 light curves in the 0.5–2 keV and 2–10 keV energy bands (top and middle panels). Time bins of 5760 s ( $\sim 1$  *Suzaku* orbit) have been used. The bottom panel shows the *Suzaku* PIN light curve in the 15–40 keV energy range; time bins are 2 satellites orbit. Given the uncertainty on the PIN background, for completeness, we have plotted both 1 (solid line) and 3  $\sigma$  (dotted lines) error bars.

of some small-amplitude variations during observation A, within each individual exposure the soft and hard count rates do not vary significantly. The lack of short-term variability is formally confirmed by a  $\chi^2$  test and by the fractional variability analysis, whose results are reported in Table 1 and Table 2, respectively.

### 3.1. *RXTE*

*RXTE* observed 3C 390.3 on 2005, January 12 and 13, when the source was in a very high brightness state: the average 2–10 keV flux was  $5.5 \times 10^{-11} \text{ erg cm}^{-2} \text{ s}^{-1}$  with a corresponding luminosity of  $4.1 \times 10^{44} \text{ erg s}^{-1}$ , which is slightly higher than the maximum value registered in the two-year *RXTE* monitoring campaign (Glozzi et al. 2006). The left panel of Figure 2 shows the light curves in the 2–6 keV (top panel;  $P_{\chi^2} = 1.5 \times 10^{-3}$ ), 2–10 keV (middle panel;  $P_{\chi^2} = 1.1 \times 10^{-4}$ ), and 6–15 keV (bottom panel;  $P_{\chi^2} = 4.9 \times 10^{-2}$ ) energy bands, respectively. Since the *RXTE* PCA is best calibrated in the 2–15 keV energy band, a direct comparison with the soft EPIC pn light curve described above cannot be performed. Nevertheless, *RXTE* allows a direct comparison in the 2–10 keV range and also the investigation of the harder X-rays up to 15 keV. On timescales of the order of 2 days, the source count rate is clearly variable in the 2–10 keV energy band (Table 1). The fact that the harder band is only marginally variable (it is variable at a 95% confidence level) can be ascribed to the lower data quality at higher energies.

### 3.2. *Suzaku*

*Suzaku* observed 3C 390.3 on 2006 December 14–16, when the source was in a brightness state similar to that observed by *XMM-Newton* 2 years earlier ( $F_{2-10 \text{ keV}} = 3.1 \times 10^{-11} \text{ erg cm}^{-2} \text{ s}^{-1}$ ). The XIS 0.5–2 keV and 2–10 keV light curves are shown in the top and middle panels of Fig. 2b. Just as with the *RXTE* PCA light curves, both XIS light curves show significant (and correlated) variability on timescales of 2 days, confirmed by a  $\chi^2$  test whose results are reported in Table 1.

The HXD PIN instrument aboard *Suzaku* offers for the first time the opportunity to investigate the variability of 3C 390.3 at harder X-ray energies. Using the latest background file, we extracted light curves in the 15–40 keV and 40–70 keV ranges; no variability was detected in the harder energy band ( $P_{\chi^2} = 0.47$ ), while significant variability ( $P_{\chi^2} = 1 \times 10^{-4}$ ) seems to be present in the 15–40 keV energy band, which is shown in the bottom panel of Fig. 2b. However, if we increase the PIN background level by applying systematic corrections at 1, 2 and 3  $\sigma$  levels, we obtain  $P_{\chi^2}$  values of  $1.6 \times 10^{-2}$ , 0.16, and 0.52, respectively. *Suzaku* observations thus indicate that there is significant variability in the energy range 0.5–10 keV, while above 15 keV the uncertainties on the HXD background prevent us from drawing strong conclusions.

In summary, on short timescales (few hours) the flux of 3C 390.3 is consistent with the hypothesis of being constant in all energy bands. On longer timescales (i.e., considering the two *XMM-Newton* observations together

TABLE 1  
FLUX VARIABILITY PROPERTIES

Date (yyyy/mm/dd)	Instrument (Satellite)	$F_{2-10\text{keV}}$ ( $\text{erg cm}^{-2} \text{s}^{-1}$ )	0.5–2 keV variability $\chi^2/\text{dof}$	$P_{\chi}^2$	2–10 keV variability $\chi^2/\text{dof}$	$P_{\chi}^2$
2004/10/10	EPIC pn (XMM)	$3.9 \times 10^{-11}$	41.08/37	0.30	47.20/37	0.12
2004/10/17	EPIC pn (XMM)	$3.4 \times 10^{-11}$	20.01/21	0.52	19.07/21	0.58
2005/01/12-13	PCA (RXTE)	$5.5 \times 10^{-11}$			58.37/24	$1.1 \times 10^{-4}$
2006/12/14-16	XIS (Suzaku)	$3.1 \times 10^{-11}$	105.24/29	$< 1 \times 10^{-6}$	42.97/29	$4.6 \times 10^{-2}$

TABLE 2  
SPECTRAL VARIABILITY PROPERTIES

Date (yyyy/mm/dd)	Instrument (Satellite)	HR variability $\chi^2/\text{dof}$	$P_{\chi}^2$	$F_{\text{var,soft}}^a$	$F_{\text{var,hard}}^b$
2004/10/10	EPIC pn (XMM)	38.92/37	0.38	$(3.6 \pm 4.3) \times 10^{-3}$	$(9.6 \pm 5.2) \times 10^{-3}$
2004/10/17	EPIC pn (XMM)	21.61/21	0.42	...	...
2005/01/12-13	PCA (RXTE)	24.22/24	0.45	$(9.3 \pm 5.2) \times 10^{-3}$	$(8.4 \pm 5.9) \times 10^{-3}$
2006/12/14-16	XIS (Suzaku)	37.7/29	0.13	$(1.9 \pm 0.2) \times 10^{-2}$	$(1.1 \pm 0.3) \times 10^{-2}$

<sup>a</sup> The soft band is 0.5–2 keV for *XMM-Newton* and *Suzaku*, whereas for *RXTE* it is 2–6 keV.

<sup>b</sup> Similarly, the hard band corresponds to 2–10 keV for *XMM-Newton* and *Suzaku*, and to 6–15 keV for *RXTE*.

or the 2-day *RXTE* and *Suzaku* coverage) the flux variability becomes significant.

#### 4. SHORT-TIME SCALE SPECTRAL VARIABILITY

In order to study the spectral variability of 3C 390.3, we use simple methods such as the variation of the hardness ratio with time and with total count rate, and the fractional variability in different energy bands. These can provide useful information without any a priori assumption about the shape of the X-ray continuum. Thus, the results from the study of these plots can be considered as “model-independent”.

To investigate the presence of spectral variability, we first apply a  $\chi^2$  test to the time series of the hardness ratio  $HR = h/s$ , where  $h = 2-10$  keV and  $s = 0.5-2$  keV for *XMM-Newton* and *Suzaku*, whereas for *RXTE*  $h = 6-15$  keV and  $s = 2-6$  keV. The results of this test are reported in Table 2 and suggest that there is no significant spectral variability on timescales of a few hours, while on a time scale of 2 days (*Suzaku* observation) marginally significant spectral variability seems to be present. It is worth noting that even between *XMM-Newton* observations A and B only marginally significant spectral variability seems to occur: the average  $HR$  increases from  $0.349 \pm 0.001$  to  $0.354 \pm 0.002$ , which is a  $2\sigma$  effect. This is a direct consequence of the fact that the soft and hard count rates vary by the same amount: they both decrease by  $\sim 12\%$  in one week (see Fig. 1).

Spectral variability can be further investigated by plotting  $HR$  versus the total count rate. Figure 3 shows the  $HR$ -count rate plots for *XMM-Newton* (left panel), *RXTE* (middle panel), and *Suzaku* (right panel), respectively. The superimposed dashed lines represent

the best-fitting straight lines, which were obtained using the routine `fitexy` (Press et al. 1997) that accounts for the errors not only on the y-axis but along the x-axis as well. Specifically, this analysis yielded:  $y = (0.38 \pm 0.02) - (0.003 \pm 0.002)x$  for *XMM-Newton*,  $y = (1.23 \pm 0.41) - (0.01 \pm 0.07)x$  for *RXTE* and  $y = (1.11 \pm 0.13) - (0.06 \pm 0.02)x$  for *Suzaku*, respectively. In summary, while *XMM-Newton* and *RXTE* observations show very flat negative slopes that are consistent with the hypothesis of constancy, *Suzaku* shows a negative trend (i.e., a steepening of the spectrum with increasing source flux) that is significant at a  $3\sigma$  level. This result is confirmed by a non-parametric Spearman test that yields a rank correlation value of  $-0.44$  and a corresponding chance probability of  $1.6 \times 10^{-2}$ .

Another simple way to quantify the spectral variability of 3C 390.3, without considering the time ordering of the values in the light curves, is based on the fractional variability parameter  $F_{\text{var}}$ . This is a commonly used measure of the intrinsic variability amplitude relative to the mean count rate, corrected for the effect of random errors, i.e.,

$$F_{\text{var}} = \frac{(\sigma^2 - \Delta^2)^{1/2}}{\langle r \rangle} \quad (1)$$

where  $\sigma^2$  is the variance,  $\langle r \rangle$  the unweighted mean count rate, and  $\Delta^2$  the mean square value of the uncertainty associated with each individual count rate. The error on  $F_{\text{var}}$ , reported in Table 2, has been estimated following Vaughan et al. (2003). For all individual observations, we computed  $F_{\text{var}}$  on the soft and hard energy bands (as defined above), since the relatively short observations and the moderately low count rate do not allow this kind of analysis on multiple narrow energy bands. The results,

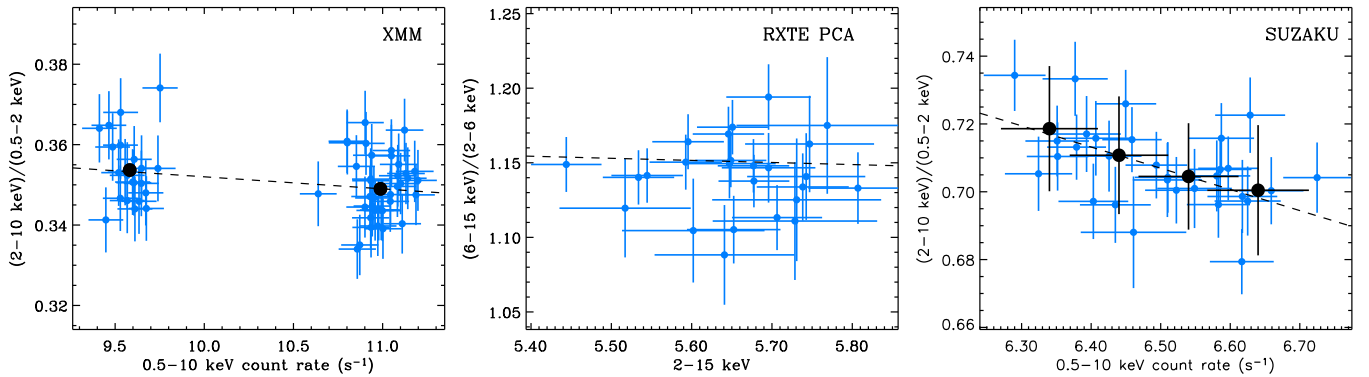


FIG. 3.— *Left:* *XMM-Newton* hardness ratio (2–10 keV)/0.5–2 keV plotted versus the total count rate. The large black circles indicate the average values during the 2 observations; the error bar is smaller than the symbols. The dashed line indicates the best linear fit. *Middle:* *RXTE* hardness ratio (6–15 keV)/2–6 keV plotted versus the total count rate. The dashed line indicates the best linear fit. *Right:* *Suzaku* XIS03 hardness ratio (2–10 keV)/0.5–2 keV plotted versus the total count rate. To guide the eye, binned values (large black circles) have been plotted over non-binned values. The dashed line indicates the best linear fit:  $y = (1.11 \pm 0.13) - (0.06 \pm 0.02)x$ .

summarized in Table 2, indicate that the variability amplitudes measured in the 2 energy bands are consistent with each other within the uncertainties. During the *Suzaku* observation there is marginal evidence ( $\sim 2.2\sigma$ ) that the soft band is more variable than the hard one.

#### 5. POWER SPECTRAL DENSITY ANALYSIS

To estimate the power-spectrum of the source in the 2–10 keV energy band we used: 1) the 1999 and 2000 *RXTE* light curve, using a 3-day bin size (“*rxte-long*” light curve, hereafter), 2) the 1996, 2-month long, *RXTE* light curve, using a 1-day bin size (“*rxte-medium*” light curve, hereafter), 3) the 2005, 2-day long, *RXTE* light curve (“*rxte-short*” light curve, hereafter), 4) the 2006, 2-day long, *Suzaku* XIS light curve, and 5) the October 10 and 17, 2004, *XMM-Newton* EPIC pn light curves. We used a 5760 s binning for the *rxte-short* and XIS light curves, and a 200 s binning for the *XMM-Newton* light curves. The October 10 2004, *XMM-Newton* light curve was split in two parts to exclude the  $\sim 2$  hours period of enhanced background activity, which was detected  $\sim 7$  hours after the start of the observation.

All light curves are evenly sampled, with a few missing points (about 5 – 10% of the total number of points). These missing points are randomly distributed over each light curve, and we accounted for them using a linear interpolation between the two bins adjacent to the gaps, adding the appropriate Poisson noise in each case.

We used equation (1) in Papadakis & Lawrence (1993) to compute the periodograms of each light curve, after normalizing them to their mean. The expected Poisson noise power level for the *rxte-long* and *rxte-medium* light curves is comparable, and for this reason we combined their periodograms in one file, and we sorted them in order of decreasing frequency (the “low-frequency” periodogram). This combined periodogram can be used for the estimation of the long and medium time scale power spectrum, from a frequency  $\sim 1/(\text{few days})$ , down to  $\sim 1/(2 \text{ years})$ . The *rxte-short* and XIS light curves also have comparable Poisson noise power level, and we therefore combined their periodograms forming the “medium-frequency” periodogram to estimate the power spectrum at higher frequencies of the order of  $\sim 1/(\text{a few hours})$ . Finally, we also combined the *XMM-Newton*

periodograms, in an attempt to detect a source signal at even higher frequencies (the “high frequency” periodogram).

Following Papadakis & Lawrence (1993), we binned the three periodograms in log-log space, using bins of size 20, and their equations (18), (19), and (20) (for the estimation of the error of the resulting binned PSD points). Our results are plotted in Fig. 4. Filled triangles indicate the high frequency PSD, estimated using the high-frequency, *XMM-Newton* periodogram. The solid line indicates the expected Poisson power level. Clearly, at frequencies higher than  $10^{-4}$  Hz, we cannot detect any intrinsic variations. The open squares in the same figure indicate the low and medium frequency PSD estimates. At low frequencies, the source PSD shows the familiar “red-noise” power spectral shape.

We fitted the low frequency PSD with a simple power-law model of the form  $P(f) \propto f^{-a}$ , taking into account the different Poisson noise power levels for the medium-frequency PSD estimate (indicated by the open square around  $f \sim 10^{-4.5}$  Hz) and the low-frequency PSD (open squares at frequencies lower than  $f \sim 10^{-5.7}$  Hz). We have also accounted for aliasing effects, as they can be estimated analytically for any given PSD model shape, following the analytical expressions in section 7.1.1 of Priestley (1989). The model describes reasonably well the PSD: the best-fit slope is  $a = 2.2 \pm 0.2$  (errors correspond to 68% confidence limits for two interesting parameters),  $\chi^2 = 12.8/6$  degrees of freedom (dof), probability of null hypothesis,  $P_{\text{null}}$ , of 4.6%. The dashed line in the left panel of Fig. 4 indicates the best-fit power-law model, and the thick solid black line, the best-fit model after taking into account the different Poisson noise power levels for the low and medium-frequency power spectra (best-fit residuals are shown in the bottom panel of the same figure). The best-fit slope is consistent with the high-frequency PSD slope detected in radio-quiet Seyfert galaxies. The steepness of the intrinsic power spectrum can explain the lack of detection of intrinsic source variations in the *XMM-Newton* light curves: the expected amplitude at the highest frequencies we can probe is much smaller than the amplitude caused by noise in the *XMM-Newton* light curves.

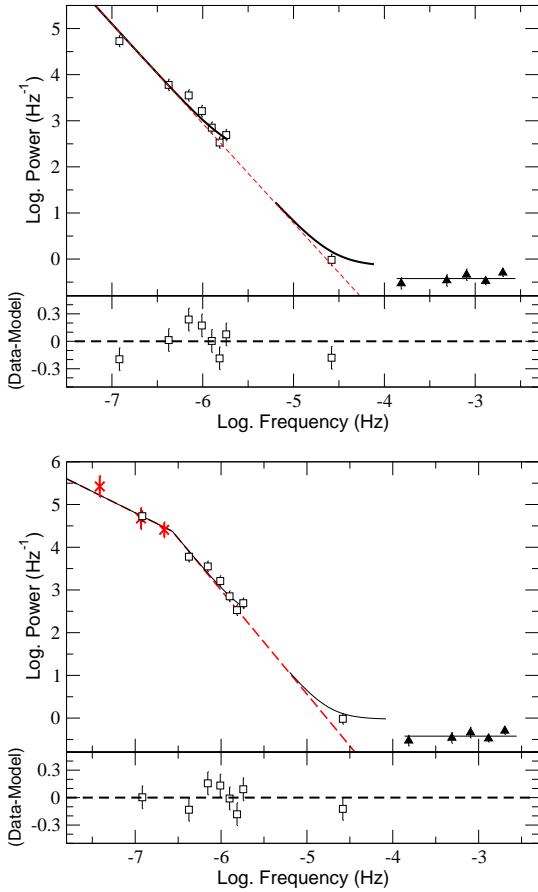


FIG. 4.— Power density spectra of 3C 390.3 based on *RXTE*, *Suzaku* (open squares), and *XMM-Newton* light curves (filled triangles) described in the text. The dashed lines indicate the best power law model fit (left panel) and the best broken power-law model fit (right panel) to the full band PSD. Solid lines indicate the best fit models when the Poisson noise power level is also taken into account. Clearly, the intrinsic power level is very low above  $10^{-4}$  Hz, hence the observed PSD in the XMM band is flat, and consistent with the predictions of a purely Poisson noise power spectrum (indicated by the solid line at the highest frequency part of the PSD).

We also tried to fit the PSD with a broken power-law model of the form:  $P(f) \propto (f/f_{\text{br}})^{-b}$ , where  $f < f_{\text{br}}$  and  $P(f) \propto (f/f_{\text{br}})^{-a}$ , at higher frequencies;  $f_{\text{br}}$  is the so called “break-frequency”. Such a model provides a good fit to the PSD of many Seyfert galaxies with  $a \sim 2$  and  $b \sim 1$  (see, e.g., Uttley, McHardy & Papadakis 2002; Papadakis et al. 2002a; Markowitz et al. 2003). Since the 3C 390.3 PSD does not show a clear slope change at low frequencies, we kept  $b$  fixed at 1, which is the typical value found in Seyfert galaxies. Note that, in case  $b$  is left free to vary, all parameters are very poorly constrained, due to paucity of data points at low frequencies. The best-fit parameters are as follows:  $a = 2.4 \pm 0.3$ ,  $f_{\text{br}} = 2.7_{-1.2}^{+3.6} \times 10^{-7}$  Hz (68% errors for 3 interesting parameters: high frequency slope, break frequency, and normalization),  $\chi^2 = 6.6/5$  dof,  $P_{\text{null}} = 25.2\%$ . The resulting best-fit model is shown in the right panel of Fig. 4 (the symbols are the same as in the left panel), and indicates that it fits the PSD very well. According to an F-test ( $F_{\text{stat}} = 4.7$ ,  $P_F = 0.082$ ),

the broken power-law model provides an improvement of the goodness of fit at a confidence level of 92%, compared to the power-law model. At the same time, the PSD plotted in the right panel of Fig. 4 indicates that the detection of this break-frequency in the power spectrum of the source is determined mainly by the lowest frequency point in the PSD. The points indicated by the crosses in the same panel, show the lowest frequency part of the power spectrum. They correspond to the 20 lowest frequency periodogram ordinates, and were estimated using bins of size 5 and 10, for the higher frequency point. These points indicate that the low frequency end of the PSD does follow a slope which is flatter than the slope of the high frequency PSD. Nevertheless, to be conservative, we consider the detection of a break-frequency in the PSD of 3C 390.3 as tentative.

## 6. DISCUSSION

In order to put our results in perspective and better understand their implications, it is important to have in mind the values of the fundamental parameters that characterize the accretion process in 3C 390.3, namely the black hole mass,  $M_{\text{BH}}$ , and the accretion rate in Eddington units,  $\dot{m}$ . To be consistent with the companion paper from Sambruna et al. (2009), in the following we assume  $M_{\text{BH}} = (5 \pm 1) \times 10^8 M_{\odot}$ , which is based on the velocity dispersion presented in Nelson et al. (2004) and is reported by Lewis & Eracleous (2006). However, for completeness and given the large uncertainties, we also consider the value obtained via reverberation mapping  $M_{\text{BH}} = (2.87 \pm 0.64) \times 10^8 M_{\odot}$  (Peterson et al. 2004). Once  $M_{\text{BH}}$  is determined,  $\dot{m}$  readily follows, by determining the bolometric luminosity,  $L_{\text{bol}}$ , and dividing it by the Eddington luminosity,  $L_{\text{Edd}} = 1.3 \times 10^{38} (M_{\text{BH}}/M_{\odot}) \text{ erg s}^{-1}$ .  $L_{\text{bol}}$  can be obtained by integrating the broadband spectral energy distribution (SED) of 3C 390.3. A detailed compilation of broadband data of 3C 390.3 ranging from the radio to the hard X-rays has been presented by Sambruna et al. (2009), yielding a bolometric luminosity in the range  $1\text{--}4 \times 10^{45} \text{ erg s}^{-1}$  (this luminosity range is a direct consequence of the long-term intrinsic variability of 3C 390.3). Combining these values with  $M_{\text{BH}}$ , we obtain an Eddington ratio ranging between 0.01 and 0.07 (0.03–0.1 for  $M_{\text{BH}} = 2.87 \times 10^8 M_{\odot}$ ), which is consistent with the lower end of the accretion rate values typically inferred in Seyfert 1 galaxies (see Vasudevan & Fabian 2009 for a recent compilation). For a source with powerful radio jets as 3C 390.3, it is also important to know the inclination angle, since beamed emission can affect any energy band including the X-rays. Based on radio data, the jet inclination angle in 3C 390.3 lies between  $30^\circ$  and  $35^\circ$  and the estimated jet velocity is  $\beta = v/c > 0.96$  (Giovannini et al. 2001). This translates into bulk Lorentz factors in the range  $\Gamma = 3.6\text{--}7.1$ , which in turn yield beaming factors in the range  $\delta \simeq 0.7\text{--}1.7$ , implying that the jet emission can be either de-beamed or beamed but in a moderate way.

The main aim of this work is to utilize the results from the short-term variability and power spectral density analyses to derive model-independent constraints on the central engine of 3C 390.3 and possibly on radio-loud AGN in general. More specifically, our findings can be used to evaluate the competing models proposed to explain the weaker X-ray reprocessing features in BLRGs,

namely dilution from the base of the jet, radiatively inefficient flow (RIAF) in the central region, or the presence of a highly ionized reflector.

### 6.1. Flux variability

Previous X-ray monitoring campaigns have shown that 3C 390.3 is highly variable on timescales ranging from several days to months. For example, using a 9-month light curve of 3C 390.3 from the *ROSAT* HRI (which probes the 0.1–2.4 keV energy band), Leighly & O’Brien (1997) demonstrated that the soft X-rays are highly variable, displaying large flares with quiescent periods in between, a behavior that and implies a non-linear nature for the variability process. Similarly, two long-term monitoring campaigns with *RXTE*, spanning respectively 3 months and 2 years, revealed that the source is highly variable also at higher X-ray energies with  $F_{\text{var}}$  ranging between 20 and 30% (Gliozzi et al. 2003a; 2006). However, since both *ROSAT* and *RXTE* are low-Earth orbit satellites the light curves were continuously interrupted, hampering the study of variability on timescales of hours.

*XMM-Newton*, with its highly elliptical orbit, has allowed the study of the short-term variability of 3C 390.3 for the first time. The EPIC light curves showed a lack of any significant short-term variability, despite the fact that the source was caught in a fairly high flux state. The lack of short-term variability lends support to the scenario where the jet does not play an important role in the X-ray emission of 3C 390.3 from 2 different points of view. First, it confirms on firmer statistical ground that 3C 390.3 follows the scaling relations typical of radio-quiet AGN that predict the short-term variability to be negligible in AGN with large  $M_{\text{BH}}$ . Second, it reveals a marked difference with respect to the typical behavior observed in jet-dominated sources, which show strong variability down to timescales of few minutes (e.g., Cui 2004). According to the current blazar paradigm, the observed short-term variability at high energies is a direct consequence of the small size of the emitting region and the observed variability timescales are further shortened by beaming effects:  $t_{\text{obs}} = t_{\text{rest}}/\delta$ . As a consequence, the lack of short-term variability in 3C 390.3 suggests that the X-ray emitting region is extended and that the beaming effects, if present, are negligible in this energy band.

The 2-day long observations carried out with *RXTE* and *Suzaku* confirm that on timescales longer than a few hours, the X-ray emission of 3C 390.3 varies significantly. Additionally, the analysis of *Suzaku* HXD-PIN data suggests a possible detection of low-amplitude flux changes up to 40 keV. However, the current uncertainties on the HXD background prevent us from drawing strong conclusions.

Important results from the temporal study can also be derived by the PSD analysis, which is the best developed timing technique and the one commonly used for investigating the time variability properties of Galactic black hole systems (GBHs) and AGN. Indeed, recent detailed PSD studies have been used to strengthen the link between GBHs and AGN (e.g., Uttley et al. 2002; Markowitz et al. 2003, McHardy et al. 2004).

The comparison of the PSD frequency break  $f_{\text{br}}$  (indicative of a characteristic timescale of the BH system) in GBHs and AGN has provided an alternative way to

determine the BH mass in AGN. McHardy et al. (2006) proposed that, in Seyfert galaxies, the break timescale,  $T_{\text{br}} = 1/f_{\text{br}}$ , scales with  $M_{\text{BH}}$  and  $L_{\text{bol}}$ , following the relationship:  $\log(T_{\text{br}}) = 2.1 \log(M_{\text{BH}}) - 0.98 \log(L_{\text{bol}}) - 2.32$ , where  $M_{\text{BH}}$  is measured in units of  $10^6 M_{\odot}$ , and  $L_{\text{bol}}$  in units of  $10^{44} \text{ erg s}^{-1}$ . Using in the above formula  $M_{\text{BH}} = 500 \times 10^6 M_{\odot}$  and  $L_{\text{bol}} = (10 - 40) \times 10^{44} \text{ erg s}^{-1}$ , obtained from the direct integration of the SED, we obtain that  $T_{\text{br}}$  ranges between 60 and 234 days (20–66 days for  $M_{\text{BH}} = 287 \times 10^6 M_{\odot}$ ). Interestingly, this result is consistent with the temporal break inferred from our PSD analysis:  $T_{\text{br}} = 43_{-25}^{+34}$  days.

McHardy and collaborators (2006) also found a tight correlation between  $T_{\text{br}}$  and the full width at half maximum (FWHM) of the  $H_{\beta}$  line:  $\log(T_{\text{br}}) = 4.20_{-0.56}^{+0.71} \times \log(\text{FWHM}(H_{\beta})) - 14.43$ . Taking into account the uncertainties on the slope, and using the value derived from our PSD analysis,  $T_{\text{br}} = 43 \text{ d}$ , the predicted  $\text{FWHM}(H_{\beta})$  for 3C 390.3 ranges between  $\sim 2000$  and  $26,000 \text{ km s}^{-1}$ , which is fully consistent with the value of  $12,700 \text{ km s}^{-1}$  derived from a time-averaged spectrum over several years (Sergeev et al. 2002).

The agreement between the predicted and the measured value of  $T_{\text{br}}$  is important in two respects. First, it lends further support to the detection of the break in the PSD of 3C 390.3. We do note that, owing to the relatively short monitoring baseline of 3C 390.3 (2 years as opposed to 5–10 years used in Seyfert studies), the detection of a break is significant only at the 92% confidence level. Nevertheless, we emphasize that this is the best estimate afforded by the current data and no improvement on the break determination will be possible in the years to come, since 3C 390.3 is not monitored by any X-ray satellite. Second, and perhaps more important, it suggests that the flux variability properties of this BLRG are indistinguishable from those of radio-quiet AGN. In contrast, PSD studies of the most prominent blazars, Mrk 421, Mrk 501, and PKS 2155 – 304 (i.e., jet-dominated AGN that have been observed with *RXTE* in long monitoring campaigns) suggest the presence of PSD breaks at frequencies that are nearly two orders of magnitude higher than the tentative break found in 3C 390.3, i.e., at  $f_{\text{br,blazar}} \simeq 10^{-5} \text{ Hz}$ , or  $T_{\text{br,blazar}} < 1 \text{ day}$  (Kataoka et al. 2001). As a consequence, the variability properties of 3C 390.3 appear to be incompatible with jet emission. On the other hand, the similarity between the variability properties of Seyfert galaxies and 3C 390.3 PSDs suggests that the X-ray variability process, and by extension the X-ray emission mechanism are similar between these two classes of object.

### 6.2. Spectral Variability

Previous studies, based on *RXTE* monitoring campaigns over periods ranging from a few months to two years, have revealed that 3C 390.3 shows correlated flux and spectral variations: the source spectrum softens as the source becomes brighter (Gliozzi et al. 2003a, 2006), which is the typical behavior observed in Seyfert galaxies (e.g., Papadakis et al. 2002b). Since these studies were performed in the 2–15 keV energy range, only our December 2005 *RXTE* observation can be formally compared with previous results. Unfortunately, due to the short duration of that observation and the limited range



of the observed flux variations (compared to the long monitoring campaigns), no significant spectral variability is detected.

Thanks to the combination of XIS0, XIS1, and XIS3 data, and their relatively low background level, the *Suzaku* light curves have higher S/N than *RXTE* and the *HR*-count rate plot clearly indicates that 3C 390.3 is consistent with the typical Seyfert-like behavior over a time interval of 2 days. It is worth noting that, unlike *RXTE* that covers only the hard X-ray range, *Suzaku* makes it possible to probe simultaneously soft (i.e.,  $E < 2$  keV) and hard energies. This is of crucial importance for BLRGs that have generally complex X-ray spectra, which cannot be fitted with a simple power law suggesting possible contributions from different physical components (see, e.g., Sambruna et al. 2009). For example, based on spectral variability results, Kataoka et al. (2007) proposed that the soft X-ray emission of 3C120 (another archetypal BLRG) was dominated by a jet.

In this context, the fact that the *Suzaku HR* – *ct* results are in full agreement with those obtained from an analogous analysis of long-term 2–15 keV *RXTE* data, suggests that also at softer energies the emission is dominated by the same Comptonized component as in Seyfert galaxies. This conclusion is further confirmed by the fact that soft (0.5–2 keV) and hard (2–10 keV) count rates appear to vary in concert (see Fig. 2 right panel). This result does not exclude the possible presence of an additional component with constant flux (such as some contribution from reflection), but it rules out the presence of a variable component, such as the beamed emission from a jet.

Further support for the latter conclusion comes from the spectral variability analysis of *XMM-Newton* data: soft and hard count rate appears to vary roughly in concert not only within each single *XMM-Newton* observation but also between the 2 *XMM-Newton* pointings that are separated in time by 1 week and in flux by 12%. At this point, one might wonder why *XMM-Newton* with its superior throughput is unable to detect a statistical significant anti-correlation in the *HR* – *ct* plot at a confidence level higher than  $2\sigma$ . The reason is simply that on short timescales (individual exposures) count rate and *HR* are constant, therefore all the information from one exposure virtually collapses to a single data point. As a consequence, the search for a negative trend in the *HR* – *ct* plot is based on 2 data points solely.

## 7. SUMMARY AND CONCLUSIONS

We have studied the short-term temporal and spectral variability properties of the BLRG 3C 390.3 using *XMM-Newton*, *RXTE*, and *Suzaku* observations carried out between October 2004 and December 2006. Our new data were then combined with older *RXTE* data obtained from long-term monitoring campaigns to investigate the PSD in detail. The main findings of our analysis can be summarized as follows:

- On short timescales (i.e., few hours, probed by uninterrupted *XMM-Newton* observations) the flux of 3C 390.3 in all energy bands is consistent with the hypothesis of being constant. On longer timescales (i.e., considering the two *XMM-Newton* observations together or the 2-day *RXTE* and *Suzaku* cov-

erage) the flux variability becomes significant.

- A detailed PSD analysis carried out over five decades in frequency suggests the presence of a break at  $T_{br} = 43_{-25}^{+34}$  days at a 92% confidence level. This is the second tentative detection of a PSD break in a radio-loud, non-jet dominated AGN, after the recent results of the BLRG 3C 120 from Marshall et al. (2009). Importantly, the time scale corresponding to the break frequency is in agreement with the relation between  $T_{br}$ ,  $M_{BH}$ , and  $L_{bol}$  as well as with the  $T_{br}$  – FWHM( $H\beta$ ) relationship, both of which are valid for Seyfert galaxies. Note that, while the relative brevity of the long-term *RXTE* campaign hampers the significance of the break detection around 40 days, the quality of the data is sufficient to rule out the presence of a break at shorter timescales, which is typically detected in PSDs of jet-dominated sources.
- The 2-day long *Suzaku* observation indicates that 3C 390.3 shows the typical spectral evolution of Seyfert galaxies in the 0.5–10 keV energy range (the spectrum becomes softer as the source brightens). This confirms previous results, based on long *RXTE* monitoring campaigns, and expands them to different energy bands and to much shorter timescales.
- The broadly coordinated variability in soft and hard X-rays during the 2-day *Suzaku* observation and between the 2 *XMM-Newton* pointings, taken one week apart, suggests a common physical origin for both energy bands, arguing against the presence of an additional variable component (i.e., a jet) emerging at softer energies.
- The lack of short-term flux variability, the frequency break of the PSD, and the Seyfert-like spectral variability consistently argue against a scenario where a jet plays a significant role in the X-ray regime, confirming the results from the time-averaged spectral analysis (Sambruna et al. 2009).

In conclusion, all our results indicate that the flux variability properties of 3C 390.3 are broadly consistent with those of radio-quiet AGN, suggesting that the X-ray variability process and, by extension, the emission mechanism in 3C 390.3 is similar to that of Seyfert galaxies. This, in turn, suggests that the weaker reflection features observed in the X-ray spectrum of 3C 390.3 are not a result of dilution by jet emission, in agreement with the conclusions of the spectral analysis of Sambruna et al. (2009). If variability studies of other BLRGs show similar results, then jet dilution will be disfavored as a general explanation of the weak reflection features in all BLRGs as a class. Of course, the jet can still influence the observed X-ray properties of BLRGs by obscuring the central regions of the accretion disk or by beaming radiation away from the disk surface. The obscuration scenario has been suggested by Sambruna et al. (2009) and Larsson et al. (2008) to account for the lack of reflection from the inner accretion disk in 3C 390.3 and 4C+74.26, respectively. Unfortunately, this scenario would also block from view the region of the accretion flow where the jet is

formed. Significant progress can be made by deep broadband observations of a large number of BLRGs so as to sample a wide variety of accretion disk geometries. The variability analysis presented here shows that, as long

as the jet angle to line of sight is large enough, such an investigation will not be subject to the effects of jet dilution.

## REFERENCES

- Ballantyne, D.R., Fabian, A.C., & Iwasawa, K. 2004, MNRAS, 354, 839  
 Ballantyne, D.R. MNRAS, 362, 1183  
 Bennet, C.L. et al. 2003, ApJS, 148, 1  
 Cui, W. 2004, ApJ, 605, 662  
 Eracleous, M., Halpern, J.P., & Livio, M. 1996, ApJ, 459, 89  
 Eracleous, M., Sambruna, R., & Mushotzky, R.F. 2000, ApJ, 537, 654  
 Giovannini, G., Cotton, W.D., Feretti, L., Lara, L., & Venturi, T. 2001, ApJ, 552, 508  
 Gliozzi, M., Sambruna, R.M., & Eracleous, M. 2003a, ApJ, 584, 176  
 Gliozzi, M., Sambruna, R.M., & Brandt, W.N. 2003b, A&A, 408, 949  
 Gliozzi, M., Papadakis, I.E., & Raeth, C. 2006, A&A, 449, 969  
 Gliozzi, M., et al. 2007, ApJ, 664, 88  
 Gliozzi, M., Foschini, L., Sambruna, R.M., & Tavecchio, F. 2008, A&A, 478, 723  
 Grandi, P., et al. 1999, A&A, 343, 33  
 Grandi, P., Malaguti, G., & Fiocchi, M. 2006, ApJ, 642, 113  
 Inda, M., et al. 1994, ApJ, 420, 143  
 Jahoda, K., Swank, J., Giles, A.B., et al. 1996, Proc.SPIE, 2808, 59  
 Kataoka, J., et al. 2001, ApJ, 560, 659  
 Kataoka, J., et al. 2007, PASJ, 59, 279  
 Larsson, J., Fabian, A.C., Ballantyne, D.R., & Miniutti, G. 2008, MNRAS, 388, 1037  
 Leighly, K.M., et al. 1997, ApJ, 483  
 Leighly, K.M. & O'Brien, P.T. 1997, ApJ, 481, L15  
 Lewis, K.T., et al. 2005, ApJ, 622, 816  
 Lewis, K.T. & Eracleous M. 2006, ApJ, 642, 711  
 Markowitz, A. et al. 2003, ApJ, 593, 96  
 Marshall, K., et al. 2009, ApJ, 696, 601  
 McHardy, I., et al. 2004, MNRAS, 348, 783  
 McHardy, I., et al. 2006, Nature, 444, 730  
 Nelson, C.H., Green, R.F., Bower, G., Gebhardt, K., & Weistrop, D. 2004, ApJ, 615, 652  
 Ogle, P.M. et al. 2004, ApJ, 618, 139  
 Papadakis, I.E. & Lawrence, A. 1993, MNRAS, 261, 612  
 Papadakis, I.E. et al. 2002a, A&A, 382, L1  
 Papadakis, I.E. et al. 2002b, ApJ, 573, 92  
 Papadakis, I.E., Ioannou, Z., Brinkmann, W., & Xilouris, E.M. 2008, A&A, 490, 995  
 Peterson, B.M., et al. 2004, ApJ, 613, 682  
 Press, W.H., Teukolsky, S.A., Vetterling, W.T., & Flannery, B.P. 1997, Numerical Recipes (Cambridge: Cambridge Univ. Press)  
 Priestley, M.B. 1989, Spectral Analysis and Time Series, Academic Press, London.  
 Rotschild, R.E., Blanco, P.R., Gruber, D.E., et al. 1998, ApJ, 496, 538  
 Sambruna, R.M., Eracleous, M., & Mushotzky, R. 1999, ApJ, 526, 60  
 Sergeev, S.G., Pronik, V.I., Peterson, B.M., Sergeeva, E.A., & Zheng, W. 2002, ApJ, 576, 660  
 Strüder, L., Briel, U., Dennerl, K., et al. 2001, A&A, 365, L18  
 Turner, M.J., Abbey, A., Arnaud, M., et al. 2001, A&A, 365, L27  
 Uttley, P., McHardy, I., & Papadakis, I.E. 2002, MNRAS, 332, 231  
 Vasudevan, R.V. & Fabian, A.C. 2008, MNRAS, 392, 1124  
 Vaughan, S., Edelson, R., Warwick, R.S., & Uttley, P. 2003, MNRAS, 345, 1271  
 Woźniak, P.R., Zdziarski, A.A., Smith, D., Madejski, G.M., & Johnson, W.N., 1998, MNRAS, 299, 449  
 Zdziarski, A.A. & Grandi, P. 2001, ApJ, 551, 186